Quantitative test of the time dependent Gintzburg-Landau equation for shearedgranular flow in two dimensions

Kuniyasu Saitoh and Hisao Hayakawa

Citation: Physics of Fluids **25**, 070606 (2013); doi: 10.1063/1.4812816
View online: http://dx.doi.org/10.1063/1.4812816
View Table of Contents: http://scitation.aip.org/content/aip/journal/pof2/25/7?ver=pdfcov
Published by the AIP Publishing

PHYSICS OF FLUIDS **25**, 070606 (2013)

Quantitative test of the time dependent Gintzburg-Landau equation for sheared granular flow in two dimensions

Kuniyasu Saitoh[1,a)] and Hisao Hayakawa[2,b)]
[1]*Faculty of Engineering Technology, University of Twente, Enschede, The Netherlands*
[2]*Yukawa Institute for Theoretical Physics, Kyoto University, Sakyo-ku, Kyoto, Japan*

(Received 25 July 2012; accepted 14 February 2013; published online 18 July 2013)

We examine the validity of the time-dependent Ginzburg-Landau equation of granular fluids for a plane shear flow under the Lees-Edwards boundary condition derived from a weakly nonlinear analysis through the comparison with the result of discrete element method. We verify quantitative agreements in the time evolution of the area fraction and the velocity fields, and also find qualitative agreement in the granular temperature. © *2013 AIP Publishing LLC*. [http://dx.doi.org/10.1063/1.4812816]

I. INTRODUCTION

Flows of granular particles have been extensively studied due to their importance in powder technology, civil engineering, mechanical engineering, geophysics, astrophysics, applied mathematics, and physics.[1–4] The characteristic properties of granular flows are mainly caused by inelastic collisions between particles.[5] In particular, studies of granular gas under a plane shear play an important role in applications of kinetic theory,[6–15] dense plugs in moderately dense flows,[16,17] long-time tail and long-range correlations,[18–27] pattern formation in dense flows,[28–33] the determination of the constitutive equation for dense flows,[34–36] as well as the jamming transition.[37–43]

The granular hydrodynamic equations based on the kinetic theory well describe the dynamics of moderately dense granular gases,[8–15] even though its applicability is questionable because of the lack of scale separation, the existence of long range correlations, etc. The two-dimensional granular shear flow is an appropriate target to check the validity of the granular hydrodynamic equations, where two denser regions are formed near the boundaries and collide to form a single dense plug under a physical boundary condition.[16,17] A similar dense plug is also observed under the Lees-Edwards boundary condition. The transient dynamics of the dense plug and the hydrodynamic fields can be described by the granular hydrodynamic equations, where reasonable agreements with the discrete element method (DEM) simulation have been verified.[17] It is also known that a homogeneous state of the two-dimensional granular shear flow is intrinsically unstable as predicted by the linear stability analysis.[44–50]

To understand the dense plug formation after the homogeneous state becomes unstable, we have to develop a weakly nonlinear analysis. Recently, Shukla and Alam carried out a weakly nonlinear analysis of the sheared granular flow in finite size systems, where they derived the Stuart-Landau equation for the disturbance amplitude of the hydrodynamic fields under a physical boundary condition.[51–55] They found the existence of subcritical bifurcation in both dilute and dense regimes, while a supercritical bifurcation appears in both medium and extremely dilute regimes. The Stuart-Landau equation, however, does not include any spatial degrees of freedom and cannot be used to study the slow evolution of dense plug. We also notice that the shear rate is fixed to unity and cannot be used as a control parameter in their analysis.

It is also notable that several authors found coexistence of solid and liquid phases in their molecular dynamics simulations of dense granular shear flows.[32,33,56–59] In particular, Khain showed

a)k.saitoh@utwente.nl. URL: http://www2.msm.ctw.utwente.nl/saitohk/.
b)hisao@yukawa.kyoto-u.ac.jp

a hysteresis loop of the order parameter defined as a density contrast between the boundary and the center region.[32,33] It should be noted, however, that the mechanism of the subcritical bifurcation based on a set of hydrodynamic equations differs from that observed in the jamming transition of frictional particles.[43] Indeed, the hysteresis loop in the jamming, which is observed for polydisperse grains, is originated from the frustrated and metastable configurations of frictional grains, while the hysteresis for monodisperse grains observed by Khain[32,33] is from the coexistence of crystal and liquid structures.

In our previous work, we have developed the weakly nonlinear analysis of the two-dimensional granular shear flow and derived the time dependent Ginzburg-Landau (TDGL) equation for the disturbance amplitude. We introduced a hybrid approach to the weakly nonlinear analysis, where the derived TDGL equation is written as a two-dimensional form and has time dependent diffusion coefficients.[60] We have also discussed the bifurcation of the amplitude. However, study of the numerical solution of the TDGL equation and comparison with DEM simulation had been left as an incomplete part of our previous paper.[60] Part of this study without comparison with DEM simulation has been published in another paper.[61]

In this paper, we quantitatively examine the validity of the derived TDGL equation for a two dimensional granular shear flow from the comparison with DEM simulation. In Sec. II, we review the weakly nonlinear analysis and the hybrid approach. In Sec. III, which is the main part of this paper, we compare the numerical solutions of the TDGL equation with the results of DEM simulation. In Sec. IV, we discuss and conclude our results.

II. OVERVIEW OF WEAKLY NONLINEAR ANALYSIS

In this section, we review our previous results of the weakly nonlinear analysis, where the time evolution of the disturbance amplitude is described by the TDGL equation.[60] We also apply the hybrid approach to the TDGL equation to describe the structural changes of the dense plug.[60] In Sec. II A, we introduce the basic equations. In Sec. II B, we review the weakly nonlinear analysis to derive the TDGL equation. In Sec. II C, we derive a two-dimensional TDGL equation adopting the hybrid approach to the weakly nonlinear analysis.

A. Basic equations

Let us explain our setup and basic equations. To avoid difficulties caused by the physical boundary condition, we adopt the Lees-Edwards boundary condition,[62] where the upper and lower image cells move to the opposite directions with a constant speed $U/2$. Here, the distance between the upper and lower image cells is given by L. We assume that the granular disks are identical, where the mass, the diameter, and the restitution coefficient are given by m, d, and e, respectively. In the following argument, we scale mass, length, and time by m, d, and $2d/U$, respectively. Therefore, the shear rate U/L is nondimensionalized as $\epsilon \equiv 2d/L$ which becomes a small parameter in the hydrodynamic limit $L \gg d$.

We employ a set of hydrodynamic equations of granular disks derived by Jenkins and Richman.[14] Although their original equations include the angular momentum and the spin temperature, it is known that the spin effects are localized near the boundary[63] and the effect of rotation can be absorbed in the normal restitution coefficient, if the friction constant is small.[17,64,65] Thus, our system is reduced to a system without the spin effects and the dimensionless hydrodynamic equations are given by

$$(\partial_t + \mathbf{v}\cdot\nabla)\,\nu = -\nu\nabla\cdot\mathbf{v}, \tag{1}$$

$$\nu\,(\partial_t + \mathbf{v}\cdot\nabla)\,\mathbf{v} = -\nabla\cdot\mathsf{P}, \tag{2}$$

$$(\nu/2)\,(\partial_t + \mathbf{v}\cdot\nabla)\,\theta = -\mathsf{P}:\nabla\mathbf{v} - \nabla\cdot\mathbf{q} - \chi, \tag{3}$$

TABLE I. The functions in Eqs. (4)–(6).

$p(\nu) = \frac{1}{2}\nu\left[1 + (1+e)\nu g(\nu)\right]$
$\xi(\nu) = \frac{1}{\sqrt{2\pi}}(1+e)\nu^2 g(\nu)$
$\eta(\nu) = \sqrt{\frac{\pi}{2}}\left[\frac{g(\nu)^{-1}}{7-3e} + \frac{(1+e)(3e+1)}{4(7-3e)}\nu + \left(\frac{(1+e)(3e-1)}{8(7-3e)} + \frac{1}{\pi}\right)(1+e)\nu^2 g(\nu)\right]$
$\kappa(\nu) = \sqrt{2\pi}\left[\frac{g(\nu)^{-1}}{(1+e)(19-15e)} + \frac{3(2e^2+e+1)}{8(19-15e)}\nu + \left(\frac{9(1+e)(2e-1)}{32(19-15e)} + \frac{1}{4\pi}\right)(1+e)\nu^2 g(\nu)\right]$
$\lambda(\nu) = -\sqrt{\frac{\pi}{2}}\frac{3e(1-e)}{16(19-15e)}\left[4(\nu g(\nu))^{-1} + 3(1+e)\right]\frac{d\left(\nu^2 g(\nu)\right)}{d\nu}$

where ν, $\mathbf{v} = (u, w)$, θ, t, and $\nabla = (\partial/\partial_x, \partial/\partial_y)$ are the area fraction, the dimensionless velocity fields, the dimensionless granular temperature, the dimensionless time, and the dimensionless gradient, respectively. The pressure tensor $\mathsf{P} = (P_{ij})$, the heat flux $\mathbf{q}$, and the energy dissipation rate χ are given in the dimensionless forms as

$$P_{ij} = \left[p(\nu)\theta - \xi(\nu)\theta^{1/2}(\nabla\cdot\mathbf{v})\right]\delta_{ij} - \eta(\nu)\theta^{1/2}e_{ij}, \tag{4}$$

$$\mathbf{q} = -\kappa(\nu)\theta^{1/2}\nabla\theta - \lambda(\nu)\theta^{3/2}\nabla\nu, \tag{5}$$

$$\chi = \frac{1-e^2}{4\sqrt{2\pi}}\nu^2 g(\nu)\theta^{1/2}\left[4\theta - 3\sqrt{\frac{\pi}{2}}\theta^{1/2}(\nabla\cdot\mathbf{v})\right], \tag{6}$$

respectively, where $p(\nu)\theta$, $\xi(\nu)\theta^{1/2}$, $\eta(\nu)\theta^{1/2}$, $\kappa(\nu)\theta^{1/2}$, and $\lambda(\nu)\theta^{3/2}$ are the dimensionless forms of the static pressure, the bulk viscosity, the shear viscosity, the heat conductivity, and the coefficient associated with the gradient of density, respectively. Here, $e_{ij} \equiv (\nabla_j v_i + \nabla_i v_j - \delta_{ij}\nabla\cdot\mathbf{v})/2(i, j = x, y)$ is the deviatoric part of the strain rate tensor. The explicit forms of them are listed in Table I, where we adopt the radial distribution function at contact

$$g(\nu) = \frac{1 - 7\nu/16}{(1-\nu)^2}, \tag{7}$$

which is only valid for $\nu < 0.7$.[66–69] A set of homogeneous solutions of Eqs. (1)–(3) is readily found as $\phi_0 \equiv (\nu_0, \epsilon y, 0, \theta_0)$, where ν_0 and θ_0 are the mean area fraction and the mean granular temperature, respectively.

B. Weakly nonlinear analysis

To study the slow dynamics of dense plug, we need to develop a weakly nonlinear analysis. For this purpose, we introduce a long time scale $\tau \equiv \epsilon^2 t$ and long length scales $(\xi, \zeta) \equiv \epsilon(x, y)$. We also introduce the neutral solution around the most unstable mode $\mathbf{q}_c = (0, q_c)$ as

$$\hat{\phi}_{\mathrm{n}} = A^{\mathrm{L}}(\zeta, \tau)\phi^{\mathrm{L}}_{q_c} e^{iq_c\zeta} + \mathrm{c.c.}, \tag{8}$$

where c.c. represents the complex conjugate and $\phi^{\mathrm{L}}_{q_c}$ corresponds to the Fourier coefficient of the hydrodynamic fields at $\mathbf{q}_c$. We notice that the amplitude of the layering mode $A^{\mathrm{L}}(\zeta, \tau)$ depends on ζ but is independent of ξ, because any non-layering modes $q_x \neq 0$ are linearly stable. Then, we expand $A^{\mathrm{L}}(\zeta, \tau)$ into the series of ϵ as

$$A^{\mathrm{L}}(\zeta, \tau) = \epsilon A^{\mathrm{L}}_1 + \epsilon^2 A^{\mathrm{L}}_2 + \epsilon^3 A^{\mathrm{L}}_3 + \ldots. \tag{9}$$

Substituting Eqs. (8) and (9) into the hydrodynamic equations (1)–(3) and collecting terms in each order of ϵ, we obtain an amplitude equation.

The first non-trivial equation at $O(\epsilon^3)$ is the TDGL equation

$$\partial_\tau A^{\mathrm{L}}_1 = \sigma_c A^{\mathrm{L}}_1 + D\partial^2_\zeta A^{\mathrm{L}}_1 + \beta A^{\mathrm{L}}_1 |A^{\mathrm{L}}_1|^2, \tag{10}$$

where D and β are listed in Table 2 of Ref. 60. Here, σ_c is the maximum growth rate at $\mathbf{q}_c$ scaled by ϵ^2. Because of the scaling relations $D = \bar{D}$ and $\beta = \epsilon\bar{\beta}$, we can rewrite Eq. (10) as the equation for the scaled amplitude $\bar{A}_1^{\mathrm{L}} \equiv \epsilon^{1/2} A_1^{\mathrm{L}}$,

$$\partial_\tau \bar{A}_1^{\mathrm{L}} = \sigma_c \bar{A}_1^{\mathrm{L}} + \bar{D}\partial_\zeta^2 \bar{A}_1^{\mathrm{L}} + \bar{\beta}\bar{A}_1^{\mathrm{L}}|\bar{A}_1^{\mathrm{L}}|^2. \tag{11}$$

It should be noted that the TDGL equation (10) or (11) can be only used for $\beta, \bar{\beta} < 0$, i.e., the case of a supercritical bifurcation.

Developing a similar procedure till $O(\epsilon^5)$, we also find the amplitude equation

$$\partial_\tau \check{A}^{\mathrm{L}} = \sigma_c \check{A}^{\mathrm{L}} + \bar{D}\partial_\zeta^2 \check{A}^{\mathrm{L}} + \bar{\beta}\check{A}^{\mathrm{L}}|\check{A}^{\mathrm{L}}|^2 + \epsilon\bar{\gamma}\check{A}^{\mathrm{L}}|\check{A}^{\mathrm{L}}|^4 + O(\epsilon^3) \tag{12}$$

for $\check{A}^{\mathrm{L}}(\zeta, \tau) = \epsilon^{1/2}[A_1^{\mathrm{L}}(\zeta, \tau) + \epsilon A_2^{\mathrm{L}}(\zeta, \tau) + \epsilon^2 A_3^{\mathrm{L}}(\zeta, \tau)]$, where $\bar{\gamma}$ is also listed in Table 2 of Ref. 60. Equation (12) can be used for $\bar{\beta} > 0$ and $\bar{\gamma} < 0$, i.e., the case of a subcritical bifurcation.

C. Hybrid approach to the weakly nonlinear analysis

Although we derived the TDGL equations (11) and (12), these equations do not include ξ and they are still not appropriate to study the two-dimensional structure of dense plug. Therefore, we need a new approach, where the non-layering mode is coupled with the layering mode. For this purpose, we add a small deviation to the most unstable mode as $\mathbf{q}(\tau) = \mathbf{q}_c + \delta\mathbf{q}(\tau)$ and assume $\hat{\phi}_{\mathrm{n}}$ does not change if the deviation $\delta\mathbf{q}(\tau)$ is small. Then, Eq. (8) can be rewritten as

$$\hat{\phi}_{\mathrm{n}} \simeq A^{\mathrm{L}}(\xi, \zeta, \tau)\phi_{q_c}^{\mathrm{L}} e^{i\mathbf{q}(\tau)\cdot\mathbf{z}} + \mathrm{c.c.}, \tag{13}$$

where we have introduced $\mathbf{z} \equiv (\xi, \zeta)$ and a ξ-dependent amplitude $A^{\mathrm{L}}(\xi, \zeta, \tau)$. If we take into account the contribution from the non-layering mode, a hybrid solution is introduced as

$$\begin{aligned}\hat{\phi}_{\mathrm{h}} &= \left\{A^{\mathrm{L}}(\xi, \zeta, \tau)\phi_{q_c}^{\mathrm{L}} + A^{\mathrm{NL}}(\xi, \zeta, \tau)\phi_{\mathbf{q}(\tau)}^{\mathrm{NL}}\right\} e^{i\mathbf{q}(\tau)\cdot\mathbf{z}} + \mathrm{c.c.} \\ &\simeq A(\xi, \zeta, \tau)\left\{\phi_{q_c}^{\mathrm{L}} + \phi_{\mathbf{q}(\tau)}^{\mathrm{NL}}\right\} e^{i\mathbf{q}(\tau)\cdot\mathbf{z}} + \mathrm{c.c.},\end{aligned} \tag{14}$$

where $A^{\mathrm{NL}}(\xi, \zeta, \tau)$ and $\phi_{\mathbf{q}(\tau)}^{\mathrm{NL}}$ are the amplitude and the Fourier coefficient of the non-layering mode, respectively. Here, we have used a strong assumption that $A^{\mathrm{L}}(\xi, \zeta, \tau)$ and $A^{\mathrm{NL}}(\xi, \zeta, \tau)$ are scaled by common amplitude $A(\xi, \zeta, \tau)$ in the second line of Eq. (14). Expanding $A(\xi, \zeta, \tau)$ as

$$A(\xi, \zeta, \tau) = \epsilon A_1(\xi, \zeta, \tau) + \epsilon^2 A_2(\xi, \zeta, \tau) + \epsilon^3 A_3(\xi, \zeta, \tau) + \ldots, \tag{15}$$

and carrying out the weakly nonlinear analysis for the hybrid solution $\hat{\phi}_{\mathrm{h}}$, we find that the rescaled amplitude $\bar{A}_1(\xi, \zeta, \tau) \equiv \epsilon^{1/2} A_1(\xi, \zeta, \tau)$ satisfies

$$\partial_\tau \bar{A}_1 = \sigma_c \bar{A}_1 + \bar{D}_1(\tau)\partial_\xi^2 \bar{A}_1 + \bar{D}_2(\tau)\partial_\xi\partial_\zeta \bar{A}_1 + \bar{D}\partial_\zeta^2 \bar{A}_1 + \bar{\beta}\bar{A}_1|\bar{A}_1|^2 \tag{16}$$

at $O(\epsilon^3)$, where $\bar{D}_1(\tau)$ and $\bar{D}_2(\tau)$ are the time dependent diffusion coefficients. Similarly, we find the higher order equation

$$\partial_\tau \check{A} = \sigma_c \check{A} + \bar{D}_1(\tau)\partial_\xi^2 \check{A} + \bar{D}_2(\tau)\partial_\xi\partial_\zeta \check{A} + \bar{D}\partial_\zeta^2 \check{A} + \bar{\beta}\check{A}|\check{A}|^2 + \epsilon\bar{\gamma}\check{A}|\check{A}|^4 + O(\epsilon^3) \tag{17}$$

for $\check{A}(\xi, \zeta, \tau) \equiv \epsilon^{1/2}\{A_1(\xi, \zeta, \tau) + \epsilon A_2(\xi, \zeta, \tau) + \epsilon^2 A_3(\xi, \zeta, \tau)\}$. The time dependent diffusion coefficients $\bar{D}_1(\tau)$ and $\bar{D}_2(\tau)$ whose explicit forms are given by Eqs. (64) and (65) in Ref. 60 decay to zero as time goes on. Therefore, Eqs. (16) and (17) are respectively reduced to Eqs. (11) and (12) in the long time limit.

III. DISCRETE ELEMENT METHOD SIMULATION

In this section, we perform the DEM simulation of a two-dimensional granular shear flow to compare the results with the weakly nonlinear analysis. In Sec. III A, we introduce our setup. In Sec. III B, we show the time evolution of the density field obtained from the DEM simulation, where the typical transient dynamics can be reproduced. In Sec. III C, we exhibit the time evolution of the velocity fields and the granular temperature. In Sec. III D, we compare the numerical solution of the TDGL equation with the DEM simulation. In the following, we use the same units of mass, length, and time as those in the weakly nonlinear analysis.

In Eq. (16), $\bar{\beta} < 0$ for $\nu_0 < 0.245$, where the supercritical bifurcation is expected.[60] If $0.245 < \nu_0 < 0.275$, $\bar{\beta} > 0$, and $\bar{\gamma} < 0$, thus Eq. (17) should be used and the subcritical bifurcation is expected. Unfortunately, $\bar{\beta} > 0$ and $\bar{\gamma} > 0$ for $\nu_0 > 0.275$ and neither Eqs. (16) nor (17) can be used. Therefore, we exhibit our numerical results with $\nu_0 = 0.18$ and 0.26 for the supercritical and subcritical cases, respectively.

A. Setup

We adopt the linear spring-dashpot model $f_n = k_n\delta - \eta_n\dot{\delta}$ for the normal force between two colliding disks, where δ, $\dot{\delta}$, k_n, and η_n are the overlap, the relative speed, the spring constant, and the viscosity coefficient, respectively. For simplicity, we ignore tangential contact forces, because we have already verified the results are unchanged for the realistic value of the friction coefficient by introducing the effective restitution coefficient.[17,65] In our simulations, we use $k_n = 500mU^2/d^2$ and $\eta_n = 1.0mU/d$. In this case, the normal restitution coefficient given by Refs. 70 and 71,

$$e = \exp\left[-\frac{\pi}{\sqrt{2mk_n/\eta_n^2 - 1}}\right], \tag{18}$$

is $e \simeq 0.9$ which may not be sufficiently large to ensure elastic limit. We adopt the periodic boundary condition and the Lees-Edwards boundary condition with the relative speed U for the boundaries of the ξ- and ζ-axes, respectively. We randomly distribute $N = 8192$ particles in $L^* \times L^*$ square boxes with the dimensionless lengths $L^* \equiv L/d = 189$ and 155 for $\nu_0 = 0.18$ and 0.26, respectively. Then, we randomly distribute the initial velocities around the linear velocity profile with the dimensionless shear rate $\epsilon \simeq 10^{-2}$.

B. Dense plug formation

Figure 1 (upper panel) displays the time evolution of disks in our DEM simulation for $\nu_0 = 0.18$. Hydrodynamic fields can be obtained by the coarse graining (CG) procedure developed by Goldhirsch *et al.*,[72–81] where the CG function is defined as $\psi(\mathbf{z}) = e^{-\mathbf{z}^2}/\pi$ at $\mathbf{z} = (\xi, \zeta)$. Figure 1 (middle panel) shows the time evolution of the area fraction defined as

$$\nu_{\rm DEM}(\mathbf{z}, \tau) = \frac{\pi}{4}\sum_{i=1}^{N}\psi(\mathbf{z} - \mathbf{z}_i), \tag{19}$$

where $\mathbf{z}_i = (\xi_i, \zeta_i)$ is the dimensionless position of ith disk. Figure 1 (lower panel) exhibits the numerical solution of Eq. (16).

In Fig. 1, a typical transient dynamics exhibits that (a) fluctuations with short wave lengths are suppressed, (b) clusters are generated and merged, and (c) a dense plug is generated and the system reaches a steady state. Such transient dynamics of dense plug is qualitatively similar to the numerical solution of Eq. (16). We should stress that these results can be explained by neither the one-dimensional TDGL equation nor the Stuart-Landau equation obtained from the ordinary weakly nonlinear analysis.[51–53]

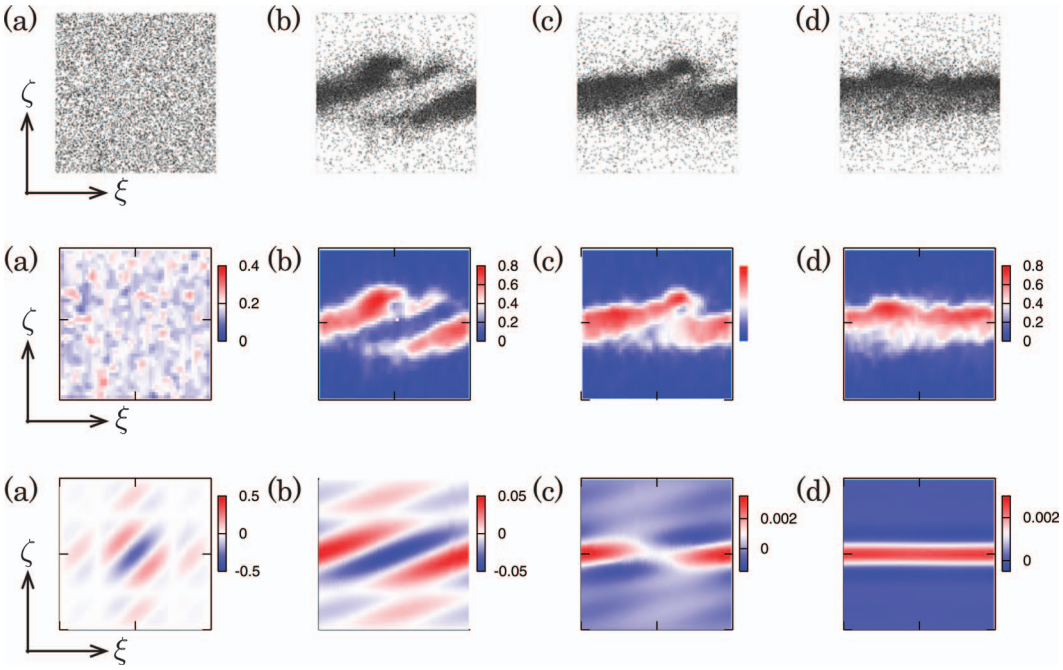

FIG. 1. (Upper panel) Time evolution of disks in the DEM simulation for $\nu_0 = 0.18$. (Middle panel) Time evolution of $\nu_{\mathrm{DEM}}(\mathbf{z}, \tau)$. (Lower panel) Numerical solution of Eq. (16). Here, $\tau =$ (a) 0, (b) 4.8, (c) 11.2, and (d) 20.0, respectively.

C. Velocity fields and granular temperature

The velocity fields and the granular temperature are defined as

$$\mathbf{u}_{\mathrm{DEM}}(\mathbf{z}, \tau) = \frac{\sum_i \mathbf{v}_i \psi(\mathbf{z} - \mathbf{z}_i)}{\sum_i \psi(\mathbf{z} - \mathbf{z}_i)}, \tag{20}$$

$$\theta_{\mathrm{DEM}}(\mathbf{z}, \tau) = \frac{\sum_i \mathbf{V}_i^2 \psi(\mathbf{z} - \mathbf{z}_i)}{2\sum_i \psi(\mathbf{z} - \mathbf{z}_i)}, \tag{21}$$

respectively, where $\mathbf{v}_i$ and $\mathbf{V}_i = \mathbf{v}_i - \mathbf{u}_{\mathrm{DEM}}(\mathbf{z}_i, \tau)$ are the dimensionless velocity and the dimensionless local velocity of ith disk, respectively. Figure 2 (upper, middle, and lower panels) displays the time evolution of $u_{\mathrm{DEM}}(\mathbf{z}, \tau)$, $w_{\mathrm{DEM}}(\mathbf{z}, \tau)$, and $\theta_{\mathrm{DEM}}(\mathbf{z}, \tau)$, respectively, where $u_{\mathrm{DEM}}(\mathbf{z}, \tau)$ and $w_{\mathrm{DEM}}(\mathbf{z}, \tau)$ are the ξ and ζ components of $\mathbf{u}_{\mathrm{DEM}}(\mathbf{z}, \tau)$, respectively. As time goes on, $u_{\mathrm{DEM}}(\mathbf{z}, \tau)$ in the ζ direction deviates from the linear profile and $w_{\mathrm{DEM}}(\mathbf{z}, \tau)$ is almost homogeneous. The time evolution of $\theta_{\mathrm{DEM}}(\mathbf{z}, \tau)$ is accompanied with $\nu_{\mathrm{DEM}}(\mathbf{z}, \tau)$, where $\theta_{\mathrm{DEM}}(\mathbf{z}, \tau)$ is lower in the dense region and higher in the dilute region.

D. Comparison of the TDGL equation with the DEM simulation

To test the quantitative validity of the TDGL equation, we compare the numerical solution with the DEM simulation. At first, we average out $\nu_{\mathrm{DEM}}(\mathbf{z}, \tau)$, $u_{\mathrm{DEM}}(\mathbf{z}, \tau)$, $w_{\mathrm{DEM}}(\mathbf{z}, \tau)$, and $\theta_{\mathrm{DEM}}(\mathbf{z}, \tau)$ over the ξ direction and take sample averages from the different 100 time steps. Then, the hydrodynamic fields are written as one-dimensional forms $\nu_{\mathrm{DEM}}(\zeta, \tau)$, $u_{\mathrm{DEM}}(\zeta, \tau)$, $w_{\mathrm{DEM}}(\zeta, \tau)$, and $\theta_{\mathrm{DEM}}(\zeta, \tau)$, respectively. Because $\nu_{\mathrm{DEM}}(\zeta, \tau)$ and $\theta_{\mathrm{DEM}}(\zeta, \tau)$ are approximately symmetric at $\zeta = 0$, we introduce the averages as

$$\bar{\nu}_{\mathrm{DEM}}(\zeta, \tau) \equiv \frac{1}{2}\{\nu_{\mathrm{DEM}}(\zeta, \tau) + \nu_{\mathrm{DEM}}(-\zeta, \tau)\} \qquad (0 < \zeta < L^*/2), \tag{22}$$

$$\bar{\theta}_{\mathrm{DEM}}(\zeta, \tau) \equiv \frac{1}{2}\{\theta_{\mathrm{DEM}}(\zeta, \tau) + \theta_{\mathrm{DEM}}(-\zeta, \tau)\} \qquad (0 < \zeta < L^*/2), \tag{23}$$

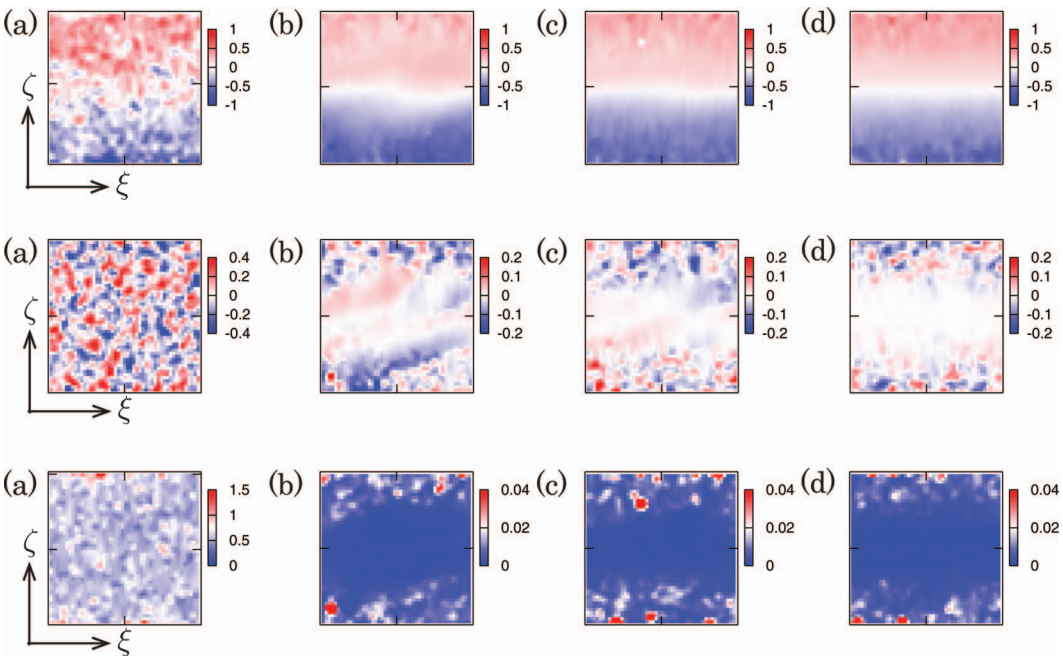

FIG. 2. Time evolution of (upper panel) $u_{\rm DEM}(\mathbf{z},\tau)$, (middle panel) $w_{\rm DEM}(\mathbf{z},\tau)$, and (lower panel) $\theta_{\rm DEM}(\mathbf{z},\tau)$. Here, $\tau =$ (a) 0, (b) 4.8, (c) 11.2, and (d) 20.0, respectively.

respectively. On the other hand, the velocity fields are approximately antisymmetric at $\zeta = 0$. Thus, we introduce the averages as

$$\bar{u}_{\rm DEM}(\zeta,\tau) \equiv \frac{1}{2}\left\{u_{\rm DEM}(\zeta,\tau) - u_{\rm DEM}(-\zeta,\tau)\right\} \qquad (0 < \zeta < L^*/2), \tag{24}$$

$$\bar{w}_{\rm DEM}(\zeta,\tau) \equiv \frac{1}{2}\left\{w_{\rm DEM}(\zeta,\tau) - w_{\rm DEM}(-\zeta,\tau)\right\} \qquad (0 < \zeta < L^*/2), \tag{25}$$

respectively.

In the weakly nonlinear analysis, the hydrodynamic fields are given by the summation of the base state $\phi_0 = (\nu_0, \zeta, 0, \theta_0)$ and the hybrid solution $\hat{\phi}_{\rm h}$. At first, we project $\hat{\phi}_{\rm h}$ on the ζ-axis as

$$\hat{\phi}_{\rm h}(\zeta,\tau) \simeq \bar{\bar{A}}(\zeta,\tau)\phi^{\rm L}_{q_c} e^{iq_\zeta(\tau)\zeta} + \text{c.c.}, \tag{26}$$

where $q_\zeta(\tau) \equiv q_c - \tau$ is the ζ component of $\mathbf{q}(\tau)$.[82] Here, we ignore $\phi^{\rm NL}_{\mathbf{q}(\tau)}$, because $\phi^{\rm NL}_{\mathbf{q}(\tau)}$ exponentially decays to zero and the following results are unchanged even if we take into account $\phi^{\rm NL}_{\mathbf{q}(\tau)}$. We note that $\phi^{\rm L}_{q_c}$ is defined as $\phi^{\rm L}_{q_c} = \left(\nu_{q_c}, iu_{q_c}, iw_{q_c}, \theta_{q_c}\right)^{\rm T}$ with the imaginary unit i, where ν_{q_c}, u_{q_c}, w_{q_c}, and θ_{q_c} are the Fourier coefficients of the area fraction, the velocity fields u and w, and the granular temperature, respectively. The explicit forms of them are given in our previous paper.[60] If we ignore the higher order terms in Eq. (15), $\bar{\bar{A}}(\zeta,\tau)$ may be given by projecting the numerical solution of Eq. (16) or (17) on the ζ-axis. Then, the hydrodynamic fields are given by $\phi_{\rm TDGL}(\zeta,\tau) = \phi_0 + \hat{\phi}_{\rm h}(\zeta,\tau)$, where each component of $\phi_{\rm TDGL}(\zeta,\tau)$ is written as

$$\nu_{\rm TDGL}(\zeta,\tau) = \nu_0 + 2\nu_{q_c}\bar{\bar{A}}(\zeta,\tau)\cos(q_\zeta(\tau)\zeta), \tag{27}$$

$$u_{\rm TDGL}(\zeta,\tau) = \zeta - 2u_{q_c}\bar{\bar{A}}(\zeta,\tau)\sin(q_\zeta(\tau)\zeta), \tag{28}$$

$$w_{\rm TDGL}(\zeta,\tau) = -2w_{q_c}\bar{\bar{A}}(\zeta,\tau)\sin(q_\zeta(\tau)\zeta), \tag{29}$$

$$\theta_{\rm TDGL}(\zeta,\tau) = \theta_0 + 2\theta_{q_c}\bar{\bar{A}}(\zeta,\tau)\cos(q_\zeta(\tau)\zeta), \tag{30}$$

respectively. Here, the factor 2 comes from the complex conjugate.

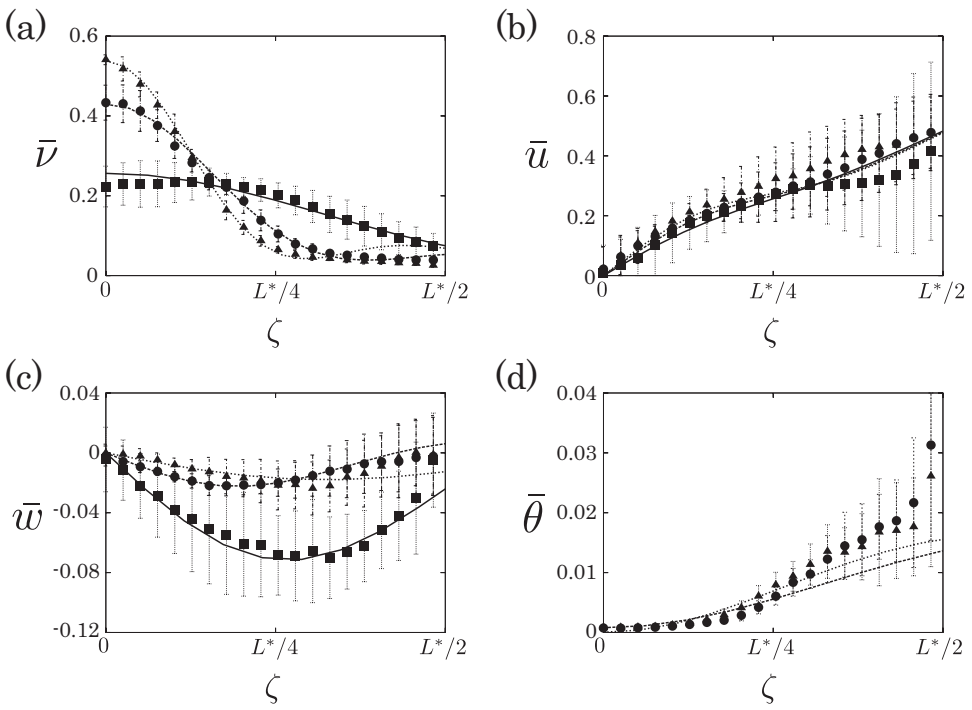

FIG. 3. Time evolution of (a) the area fraction, (b) the ξ- and (c) ζ-components of the velocity field, and (d) the granular temperature for the supercritical case ($\nu_0 = 0.18$), where the solid squares, circles, and triangles represent $\bar{X}_{\rm DEM}(\zeta, \tau)$ ($X = \nu, u, w, \theta$) at $\tau = 4.8$, 11.2, and 20.0, respectively. The solid, hashed, and dotted lines are $\bar{X}_{\rm TDGL}(\zeta, \tau)$ ($X = \nu, u, w, \theta$) at $\tau = 4.8$, 11.2, and 20.0, respectively. Here, the scaling factors are introduced as $\tau^* \simeq 0.14$, $a_\nu^* \simeq 0.24$, $a_u^* \simeq 0.02$, $a_w^* \simeq 1.96$, and $a_\theta^* \simeq 0.02$, respectively. We also use $\zeta_\nu^*(\tau) \simeq 1.6, 0.9, 0.75$, $\zeta_u^*(\tau) \simeq 0.8, 0.8, 0.8$, and $\zeta_w^*(\tau) \simeq 1.5, 1.1, 1.8$ at $\tau = 4.8$, 11.2, and 20.0, respectively, and $\zeta_\theta^*(\tau) \simeq 1.6, 1.35$ at $\tau = 11.2$ and 20.0, respectively. It should be noted that we do not show the result of the granular temperature at $\tau = 4.8$, because it homogeneously distributes around θ_0 and its fluctuation is too large to plot in the same figure. The relative standard deviations are Err. $\simeq$ (a) 0.09, (b) 0.07, (c) 0.10, and (d) 0.35, respectively.

Figures 3 and 4 display the time evolution of the hydrodynamic fields for the supercritical ($\nu_0 = 0.18$) and subcritical ($\nu_0 = 0.26$) cases, respectively, where the symbols represent Eqs. (22)–(25) and the lines represent the scaling functions

$$\bar{X}_{\rm TDGL}(\zeta, \tau) \equiv a_X^* X_{\rm TDGL}(\zeta/\zeta_X^*(\tau), \tau/\tau^*) \quad (X = \nu, u, w, \theta), \tag{31}$$

with the scaling factors a_X^*, $\zeta_X^*(\tau)$ and τ^*. We quantify the difference between Eqs. (22)–(25) and Eq. (31) by introducing the relative standard deviation

$$\text{Err.} \equiv \sqrt{\frac{\left(\bar{X}_{\rm DEM} - \bar{X}_{\rm TDGL}\right)^2}{\bar{X}_{\rm TDGL}^2}} \quad (X = \nu, u, w, \theta), \tag{32}$$

where we omit the arguments (ζ, τ). In Figs. 3(a)–3(c), $\bar{\nu}_{\rm TDGL}(\zeta, \tau)$, $\bar{u}_{\rm TDGL}(\zeta, \tau)$, and $\bar{w}_{\rm TDGL}(\zeta, \tau)$ quantitatively agree with $\bar{\nu}_{\rm DEM}(\zeta, \tau)$, $\bar{u}_{\rm DEM}(\zeta, \tau)$, and $\bar{w}_{\rm DEM}(\zeta, \tau)$, respectively, where Err. is less than or equal to 0.1. In Figs. 4(a) and 4(b), $\bar{\nu}_{\rm TDGL}(\zeta, \tau)$ and $\bar{u}_{\rm TDGL}(\zeta, \tau)$ quantitatively agree with $\bar{\nu}_{\rm DEM}(\zeta, \tau)$ and $\bar{u}_{\rm DEM}(\zeta, \tau)$, respectively. We should note that we could not get any reasonable agreements between the ζ component of the velocity field obtained from the DEM simulation under the physical boundary condition and the numerical solution of the set of granular hydrodynamic equations in our previous work.[17] We can also confirm the qualitative agreements in the ζ component of the velocity field for the subcritical case (Fig. 4(c)) and the granular temperature for both the supercritical and subcritical cases (Figs. 3(d) and 4(d)), where Err. is less than or equal to 0.43.

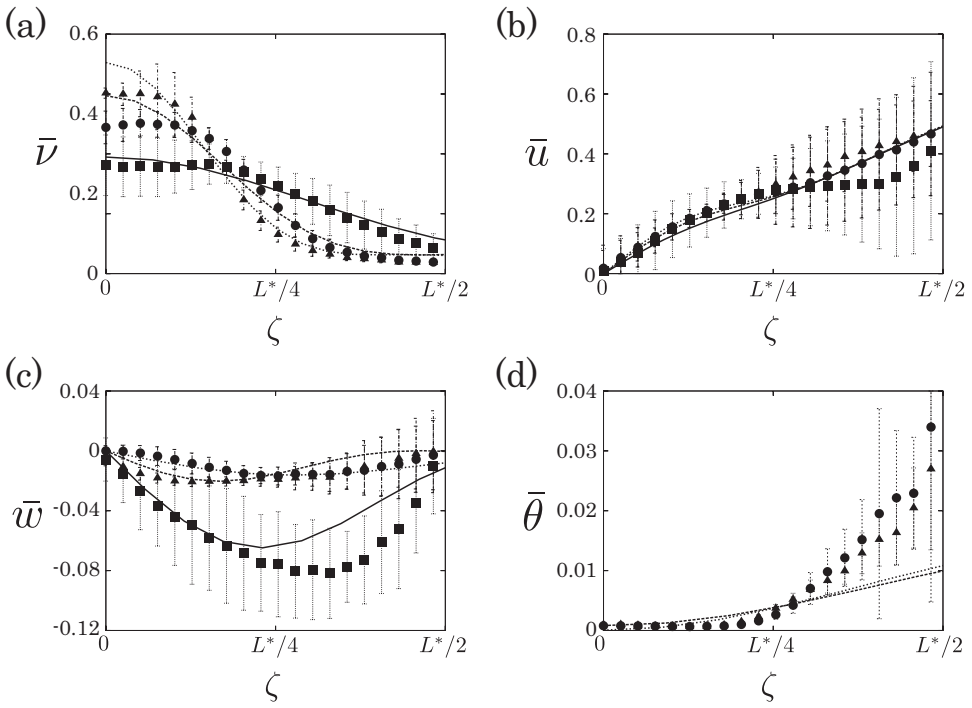

FIG. 4. Time evolution of (a) the area fraction, (b) the ξ- and (c) ζ-components of the velocity field, and (d) the granular temperature for the subcritical case ($v_0 = 0.26$), where we use the same sets of τ and scaling factors used in Fig. 3. Here, the relative standard deviations are Err. $\simeq$ (a) 0.10, (b) 0.07, (c) 0.40, and (d) 0.43, respectively.

IV. DISCUSSION AND CONCLUSION

In this paper, we examine the validity of the TDGL equation for a two-dimensional sheared granular flow from the comparison with the DEM simulation. The results of the TDGL equation, at least, qualitatively agree with the results of the DEM simulation. Such transient dynamics can be reproduced by neither the one-dimensional TDGL equation nor the Stuart-Landau equation derived from the ordinary weakly nonlinear analysis.

We compare the one dimensional hydrodynamic fields obtained from the DEM simulation with the scaled forms of the numerical solution of the TDGL equation, where we find the quantitative agreements in the area fraction and the ξ component of the velocity field. In the supercritical regime, we also find the quantitative agreement in the ζ component of the velocity field. We can also observe the qualitative agreements in the ζ component of the velocity field for the subcritical case and the granular temperature for both the supercritical and subcritical cases. In our previous work, the hydrodynamic fields obtained from the DEM simulation are reasonably explained by the numerical solutions of the granular hydrodynamic equations by Jenkins and Richman except for $w(\mathbf{z}, \tau)$.[14,15,17] In the present work, even though we need to introduce the scaling factors, the results of the DEM simulation is qualitatively reproduced by the numerical solution of the TDGL equation. It is needless to say that more precise analyses will be important to remove the scaling factors. In addition, quantitative comparison with the DEM simulations in quasi elastic limit should be performed in our future studies.

In conclusion, the numerical solution of the TDGL equation can qualitatively explain the time evolution of the hydrodynamic fields obtained from the DEM simulation.

ACKNOWLEDGMENTS

This work was financially supported by an NWO-STW VICI grant. Numerical computation in this work was carried out at the Yukawa Institute Computer Facility.

[1] S. Luding, "Towards dense, realistic granular media in 2d," Nonlinearity **22**, R101 (2009).
[2] *Granular Gases*, edited by T. Pöschel and S. Luding (Springer-Verlag, Berlin, 2001).
[3] N. V. Brilliantov and T. Pöschel, *Kinetic Theory of Granular Gases* (Oxford University Press, Oxford, 2004).
[4] I. Goldhirsch, "Rapid granular flows," Annu. Rev. Fluid Mech. **35**, 267 (2003).
[5] H. M. Jeager, S. R. Nagel, and R. P. Behringer, "Granular solids, liquids, and gases," Rev. Mod. Phys. **68**, 1259 (1996).
[6] N. Sela, I. Goldhirsch, and S. H. Noskowicz, "Kinetic theoretical study of a simply sheared two-dimensional granular gas to burnett order," Phys. Fluids **8**, 2337 (1996).
[7] A. Santos, V. Garzó, and J. W. Dufty, "Inherent rheology of a granular fluid in uniform shear flow," Phys. Rev. E **69**, 061303 (2004).
[8] C. K. K. Lun, "Kinetic theory for granular flow of dense, slightly inelastic, slightly rough spheres," J. Fluid Mech. **233**, 539 (1991).
[9] J. J. Brey, J. W. Dufty, C. S. Kim, and A. Santos, "Hydrodynamics for granular flow at low density," Phys. Rev. E **58**, 4638 (1998).
[10] V. Garzó and J. W. Dufty, "Dense fluid transport for inelastic hard spheres," Phys. Rev. E **59**, 5895 (1999).
[11] J. F. Lutsko, "Rheology of dense polydisperse granular fluids under shear," Phys. Rev. E **70**, 061101 (2004).
[12] J. F. Lutsko, "Transport properties of dense dissipative hard-sphere fluids for arbitrary energy loss models," Phys. Rev. E **72**, 021306 (2005).
[13] J. F. Lutsko, "Chapman-Enskog expansion about nonequilibrium states with application to the sheared granular fluid," Phys. Rev. E **73**, 021302 (2006).
[14] J. T. Jenkins and M. W. Richman, "Kinetic theory for plane flows of a dense gas of identical, rough, inelastic, circular disks," Phys. Fluids **28**, 3485 (1985).
[15] J. T. Jenkins and M. W. Richman, "Grad's 13-moment system for a dense gas of inelastic spheres," Arch. Ration. Mech. Anal. **87**, 355 (1985).
[16] M. L. Tan and I. Goldhirsch, "Intercluster interactions in rapid granular shear flows," Phys. Fluids **9**, 856 (1997).
[17] K. Saitoh and H. Hayakawa, "Rheology of a granular gas under a plane shear," Phys. Rev. E **75**, 021302 (2007).
[18] V. Kumaran, "Velocity autocorrelations and viscosity renormalization in sheared granular flows," Phys. Rev. Lett. **96**, 258002 (2006).
[19] V. Kumaran, "Dynamics of a dilute sheared inelastic fluid: Hydrodynamic modes and velocity correlation functions," Phys. Rev. E **79**, 011301 (2009).
[20] V. Kumaran, "Dynamics of a dilute sheared inelastic fluid: The effect of correlations," Phys. Rev. E **79**, 011302 (2009).
[21] A. V. Orpe and A. Kudrolli, "Velocity correlations in dense granular flows observed with internal imaging," Phys. Rev. Lett. **98**, 238001 (2007).
[22] A. V. Orpe, V. Kumaran, K. Reddy, and A. Kudrolli, "Fast decay of the velocity autocorrelation function in dense shear flow of inelastic hard spheres," Europhys. Lett. **84**, 64003 (2008).
[23] C. H. Rycroft, A. V. Orpe, and A. Kudrolli, "Physical test of a particle simulation model in a sheared granular system," Phys. Rev. E **80**, 031305 (2009).
[24] J. F. Lutsko and J. W. Dufty, "Hydrodynamic fluctuations at large shear rate," Phys. Rev. A **32**, 3040 (1985).
[25] M. Otsuki and H. Hayakawa, "Unified description of long-time tails and long-range correlation functions for sheared granular liquids," Eur. Phys. J. Spec. Top. **179**, 179 (2009).
[26] M. Otsuki and H. Hayakawa, "Spatial correlations in sheared isothermal liquids: From elastic particles to granular particles," Phys. Rev. E **79**, 021502 (2009).
[27] M. Otsuki and H. Hayakawa, "Long-time tails in sheared fluids," J. Stat. Mech.: Theory Exp. (**2009**) L08003.
[28] M. Y. Louge, "Computer simulations of rapid granular flows of spheres interacting with a flat, frictional boundary," Phys. Fluids **6**, 2253 (1994).
[29] M. Y. Louge, "Model for dense granular flows down bumpy inclines," Phys. Rev. E **67**, 061303 (2003).
[30] H. Xu, A. P. Reeves, and M. Y. Louge, "Measurement errors in the mean and fluctuation velocities of spherical grains from a computer analysis of digital images," Rev. Sci. Instrum. **75**, 811 (2004).
[31] H. Xu, M. Y. Louge, and A. P. Reeves, "Solutions of the kinetic theory for bounded collisional granular flows," Continuum Mech. Thermodyn. **15**, 321 (2003).
[32] E. Khain, "Hydrodynamics of fluid-solid coexistence in dense shear granular flow," Phys. Rev. E **75**, 051310 (2007).
[33] E. Khain, "Bistability and hysteresis in dense shear granular flow," Europhys. Lett. **87**, 14001 (2009).
[34] G. D. R. Midi, "On dense granular flows," Eur. Phys. J. E **14**, 341 (2004).
[35] F. da Cruz, S. Eman, M. Prochnow, J. N. Roux, and F. Chevoir, "Rheophysics of dense granular materials: Discrete simulation of plane shear flows," Phys. Rev. E **72**, 021309 (2005).
[36] T. Hatano, "Power-law friction in closely packed granular materials," Phys. Rev. E **75**, 060301(R) (2007).
[37] M. van Hecke, "Jamming of soft particles: Geometry, mechanics, scaling and isostaticity," J. Phys. Condens. Matter **22**, 033101 (2010).
[38] T. Hatano, M. Otsuki, and S. Sasa, "Criticality and scaling relations in a sheared granular material," J. Phys. Soc. Jpn. **76**, 023001 (2007).
[39] T. Hatano, "Scaling properties of granular rheology near the jamming transition," J. Phys. Soc. Jpn. **77**, 123002 (2008).
[40] M. Otsuki and H. Hayakawa, "Universal scaling for the jamming transition," Prog. Theor. Phys. **121**, 647 (2009).

[41] M. Otsuki and H. Hayakawa, "Critical behaviors of sheared frictionless granular materials near the jamming transition," Phys. Rev. E **80**, 011308 (2009).
[42] M. Otsuki, H. Hayakawa, and S. Luding, "Divergence of pressure and viscosity for hard and soft granular materials," Prog. Theor. Phys. Suppl. **184**, 110 (2010).
[43] M. Otsuki and H. Hayakawa, "Critical scaling near jamming transition for frictional granular particles," Phys. Rev. E **83**, 051301 (2011).
[44] S. B. Savage, "Instability of unbounded uniform granular shear flow," J. Fluid Mech. **241**, 109 (1992).
[45] V. Garzó, "Transport coefficients for an inelastic gas around uniform shear flow: Linear stability analysis," Phys. Rev. E **73**, 021304 (2006).
[46] P. J. Schmid and H. K. Kytömaa, "Transient and asymptotic stability of granular shear flow," J. Fluid Mech. **264**, 255 (1994).
[47] C.-H. Wang, R. Jackson, and S. Sundaresan, "Stability of bounded rapid shear flows of a granular material," J. Fluid Mech. **308**, 31 (1996).
[48] M. Alam and P. R. Nott, "The influence of friction on the stability of unbounded granular shear flow," J. Fluid Mech. **343**, 267 (1997).
[49] M. Alam and P. R. Nott, "Stability of plane couette flow of a granular material," J. Fluid Mech. **377**, 99 (1998).
[50] B. Gayen and M. Alam, "Algebraic and exponential instabilities in a sheared micropolar granular fluid," J. Fluid Mech. **567**, 195 (2006).
[51] P. Shukla and M. Alam, "Landau-type order parameter equation for shear banding in granular couette flow," Phys. Rev. Lett. **103**, 068001 (2009).
[52] P. Shukla and M. Alam, "Weakly nonlinear theory of shear-banding instability in a granular plane couette flow: Analytical solution, comparison with numerics and bifurcation," J. Fluid Mech. **666**, 204 (2011).
[53] P. Shukla and M. Alam, "Nonlinear stability and patterns in granular plane couette flow: Hopf and pitchfork bifurcations, and evidence for resonance," J. Fluid Mech. **672**, 147 (2011).
[54] M. Alam and P. Shukla, "Origin of subcritical shear-banding instability in a dense two-dimensional sheared granular fluid," Granular Matter **14**, 221 (2012).
[55] M. Alam, "Nonmodal stability and optimal perturbations in unbounded granular shear flow: Three-dimensionality and particle spin," Prog. Theor. Phys. Suppl. **195**, 78 (2012).
[56] M. Alam and S. Luding, "First normal stress difference and crystallization in a dense sheared granular fluid," Phys. Fluids **15**, 2298 (2003).
[57] M. Alam, V. H. Arakeri, P. R. Nott, J. D. Goddard, and H. J. Herrmann, "Instability-induced ordering, universal unfolding and the role of gravity in granular couette flow," J. Fluid Mech. **523**, 277 (2005).
[58] M. Alam, P. Shukla, and S. Luding, "Universality of shear-banding instability and crystallization in sheared granular fluid," J. Fluid Mech. **615**, 293 (2008).
[59] P. R. Nott, M. Alam, K. Agrawal, R. Jackson, and S. Sundaresan, "The effect of boundaries on the plane couette flow of granular materials: A bifurcation analysis," J. Fluid Mech. **397**, 203 (1999).
[60] K. Saitoh and H. Hayakawa, "Weakly nonlinear analysis of two dimensional sheared granular flow," Granular Matter **13**, 697 (2011).
[61] K. Saitoh and H. Hayakawa, "Time dependent Ginzburg-Landau equation for sheared granular flow," AIP Conf. Proc. **1501**, 1001 (2012).
[62] A. W. Lees and S. F. Edwards, "The computer study of transport processes under extreme conditions," J. Phys. C **5**, 1921 (1972).
[63] N. Mitarai, H. Hayakawa, and H. Nakanishi, "Collisional granular flow as a micropolar fluid," Phys. Rev. Lett. **88**, 174301 (2002).
[64] J. T. Jenkins and C. Zhang, "Kinetic theory for identical, frictional, nearly elastic spheres," Phys. Fluids **14**, 1228 (2002).
[65] D. K. Yoon and J. T. Jenkins, "Kinetic theory for identical, frictional, nearly elastic disks," Phys. Fluids **17**, 083301 (2005).
[66] L. Verlet and D. Levesque, "Integral equations for classical fluids. III. The hard discs system," Mol. Phys. **46**, 969 (1982).
[67] D. Henderson, "Monte Carlo and perturbation theory studies of the equation of state of the two-dimensional Lennard-Jones fluid," Mol. Phys. **34**, 301 (1977).
[68] D. Henderson, "A simple equation of state for hard discs," Mol. Phys. **30**, 971 (1975).
[69] N. F. Carnahan and K. E. Starling, "Equation of state for nonattracting rigid spheres," J. Chem. Phys. **51**, 635 (1969).
[70] S. Luding, "Cohesive, frictional powders: Contact models for tension," Granular Matter **10**, 235 (2008).
[71] S. Luding, "Anisotropy in cohesive, frictional granular media," J. Phys.: Condens. Matter **17**, S2623 (2005).
[72] B. J. Glasser and I. Goldhirsch, "Scale dependence, correlations, and fluctuations of stresses in rapid granular flows," Phys. Fluids **13**, 407 (2001).
[73] C. Goldenberg and I. Goldhirsch, "Force chains, microelasticity, and macroelasticity," Phys. Rev. Lett. **89**, 084302 (2002).
[74] I. Goldhirsch and C. Goldenberg, "On the microscopic foundations of elasticity," Eur. Phys. J. E **9**, 245 (2002).
[75] C. Goldenberg and I. Goldhirsch, "Small and large scale granular statics," Granular Matter **6**, 87 (2004).
[76] C. Goldenberg and I. Goldhirsch, "Friction enhances elasticity in granular solids," Nature (London) **435**, 188 (2005).
[77] C. Goldenberg, A. P. F. Atman, P. Claudin, G. Combe, and I. Goldhirsch, "Scale separation in granular packings: Stress plateaus and fluctuations," Phys. Rev. Lett. **96**, 168001 (2006).
[78] I. Goldhirsch, "Stress, stress asymmetry and couple stress: From discrete particles to continuous fields," Granular Matter **12**, 239 (2010).

[79] J. Zhang, R. P. Behringer, and I. Goldhirsch, "Coarse-graining of a physical granular system," Prog. Theor. Phys. Suppl. **184**, 16 (2010).
[80] A. H. Clark, P. Mort, and R. P. Behringer, "Coarse graining for an impeller-driven mixer system," Granular Matter **14**, 283 (2012).
[81] T. Weinhart, A. R. Thornton, S. Luding, and O. Bokhove, "From discrete particles to continuum fields near a boundary," Granular Matter **14**, 289 (2012).
[82] Here, $\mathbf{q}(\tau) = \mathbf{q}_c + \delta\mathbf{q}(\tau) \equiv (\delta q, q_c - \epsilon t \delta q)$ and we use $\delta q \sim \epsilon$, thus the ζ component of $\mathbf{q}(\tau)$ is given by $q_\zeta(\tau) = q_c - \tau$.